AUTOMATED ADAPTIVE FORMING SIMULATIONS

Jie Wan, Suleyman Kocak and Mark S. Shephard

Scientific Computation Research Center, Rensselaer Polytechnic Institute, Troy, NY, U.S.A.
shephard@scorec.rpi.edu

ABSTRACT

In this study, an automated adaptive mesh control scheme, based on local mesh modifications, is developed for the finite element simulations of 3D metal forming processes. Error indicators are used to control the mesh discretization errors, and a consecutive *h*-adaptive procedure is conducted. The mesh size field used in the *h*-adaptive procedure is processed to control the geometric approximation errors on the evolving workpiece boundary mesh. During the simulations the workpiece mesh is adaptively enriched whenever the mesh is no longer acceptable. Industrial problems are investigated to demonstrate the capabilities of the developed scheme.

Keywords: adaptive mesh control, metal forming, mesh adaptation

1. INTRODUCTION

The manufacturing and testing process of aerospace components is expensive and difficult. Mathematical modeling tools have been developed to reduce/replace the historic trial and error process. As a mathematical tool, the finite element method has been widely used to simulate metal forming problems like forging, extrusion, rolling, etc., where the mesh of the workpiece evolves to represent the material flow. These processes often require the mesh of the deformed workpiece to be enriched whenever the mesh becomes unacceptable due to severe distortion or workpiece-die interference occurring during the incremental flow process. In these cases, it is necessary to replace the deformed mesh with an updated mesh, which is better-conditioned and consistent with the current configuration [1-5]. History dependent state variables also need to be accurately transferred from the old mesh to the new mesh [1,3].

Most procedures developed to update the deformed mesh of the workpiece apply automatic mesh generation techniques to generate a completely new mesh [1-9]. Typically, a remeshing process includes the following steps: 1) Update the boundary mesh representation; 2) Generate a new mesh; and 3) Transfer the history-dependent field variables from the old mesh to the new mesh. In remeshing process, the entire domain of the workpiece is remeshed, even though there might be only a limited number of elements that need to be modified. The workload in this process could be decreased significantly by applying local modification operators.

The emphasis of the developed procedures is the effective enrichment of the deformed mesh. The mesh enrichment process is carried out by applying local mesh modification operators. An adaptive procedure built on discretization error indicators is used for the calculation of the mesh size field. In addition the mesh size field is modified to help control geometric approximation errors in the next set of simulation steps. The simulation process is automated by combining the adaptive mesh control procedure with the forming analysis engine to enable continuous automated simulation.

This paper is organized as follows: An overview of adaptive mesh modification for evolving geometries is given in Section 2. The model topology update process is discussed in Section 3. Section 4 is dedicated to definition of the mesh size field. The controlled mesh modification process is explained in Section 5. Example problems from industrial applications are given in Section 6, and finally some conclusions are drawn in Section 7.

2. OVERVIEW OF ADAPTIVE MESH MODIFICATION FOR EVOLVING GEOMETRY PROBLEMS

In metal forming simulations, the workpiece undergoes large plastic deformation that results in major changes in the geometry of the model and the mesh. Mesh enrichments are usually needed due to two reasons (i) element shapes degrade or (ii) discretization errors become too large. In the updated mesh, it is the quality of elements that determines how many time steps can be taken before the next mesh enrichment is needed. For this reason, special care is given to the mesh enrichment process.

DEFORM^{TM} [10] is the FEM engine used in this effort. DEFORM is tailored for large deformation modeling, and it can analyze various forming and heat transfer processes. The formulation of the engine is given in Kobayashi et al. [11]. The engine supports rigid, elastic and thermo-viscoplastic material models, and it has an extensive material database for many alloys.

Mesh enrichment process used in this study includes the following steps:

Update the model topology: During the simulation steps the geometry and topology (in terms of contact surfaces) of the workpiece model evolve. Therefore, a consistent model topology must be constructed before mesh modifications. In this study, the model is defined as a non-manifold topological model that reflects the contact configuration as it evolves during the simulation.

Determine the new mesh size field: Mesh modifications are conducted based on the mesh size field. In this study, the mesh size field is determined by an *h*-adaptive procedure guided by error indicators and geometric approximation control.

Apply mesh modification operations: Once the mesh size field is obtained, the mesh is modified by using local mesh modification operations. History dependent solution fields are also transferred incrementally during these operations.

3. MODEL TOPOLOGY UPDATE

In a forming simulation, the geometrical components consist of the workpiece geometry, die geometries and die motions. To properly perform an automated forming simulation, a topological description of the evolving workpiece boundary must be available to reflect the simulation status so that the workpiece boundary and the analysis attributes are appropriately maintained during the mesh updating.

Since a FEM engine will only track nodal contact information, a procedure is needed to update the topological representation of the workpiece boundary before each mesh enrichment step. The mesh model to be constructed needs to provide a consistent geometric interpretation of the contact boundary conditions between the workpiece mesh and the die surfaces, which are extracted from the solution information in terms of nodal contact. The radial edge topology structure [12,13] given in Figure 1 is used to express the topological model of the workpiece domain.

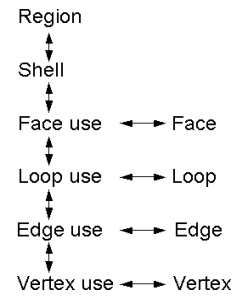

Figure 1. The radial edge topology structure for model

Given the mesh topology [14] and nodal contact conditions, mesh model construction steps can be summarized as follows with the aid of Figures 2-4, where ○ represents a mesh vertex in contact and □ represents a mesh vertex not in contact, and $M_i^{d_i}[G_C^2$ indicates a boundary mesh entity classified in contact and $M_i^{d_i}[G_F^2$ indicates a boundary mesh entity classified not in contact:

1. All boundary mesh vertices are marked according to the nodal contact conditions. The markings reflect if the mesh vertices are in contact with the specific die surfaces;
2. For each boundary mesh face, mark it in contact if all its bounding mesh vertices are in contact with the same die surface, or not in contact otherwise. The markings of boundary mesh faces are illustrated in Figure 2;
3. Consider next the boundary mesh edges. If such a mesh edge bounds only one contact mesh face, or does not bound any contact mesh faces but its two bounding mesh vertices are in contact with the same die surface, classify it on a model edge G_j^1; otherwise classify it on a model face G_j^2. Classifications of boundary mesh edges are illustrated in Figure 3, where the thickest lines indicate the mesh edges classified on model edges;
4. Consider each boundary mesh vertex. If it is marked in contact and does not bound any mesh edges classified in contact with a die surface, classify it on a model vertex G_j^0; otherwise count the number of its adjacent model edge classified mesh edges. In the latter case, if the number is 1 or greater than 2, classify it on a model vertex G_j^0; or if the number equals to 2, classify it on a model edge G_j^1. In other cases, classify it on a model face G_j^2. Classifications of boundary mesh vertices are illustrated in Figure 4;

5. Model edges are defined by the appropriate collecting of mesh edges classified on model edges that connect together;

6. Model faces are defined by collecting of mesh faces classified in contact with specific die surfaces or on the free surfaces that are bounded by loops of model edges.

When the essential boundary conditions are applied, additional care is needed so that the model topology defined also reflects those boundary conditions.

The above process naturally results in a mesh model, in which all mesh entities $M_i^{d_i}[G_j^{d_j}$ classified on a specific model entity $G_j^{d_j}$, where $d_i \le d_j \le 2$, have the identical boundary conditions. This enables the automatic maintenance and delivery of contact (and other BC's if defined) for the workpiece mesh during the local mesh modifications applied on the workpiece boundary. A mesh model constructed is shown in Figure 5, where a single shell consisting of 3 contact model faces and 1 free model face is defined (the third contact model face is at the bottom). All mesh entities, M_i^d where $0 \le d \le 2$, classified on any contact model face and its closure, are in contact with the same die surface.

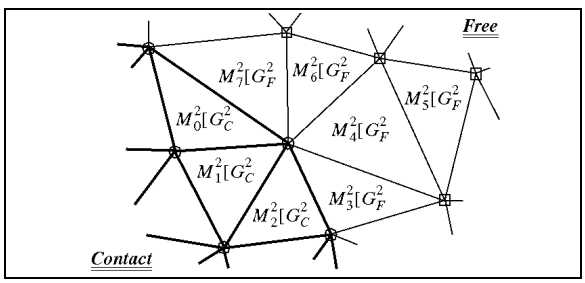

Figure 2. Marking boundary mesh faces

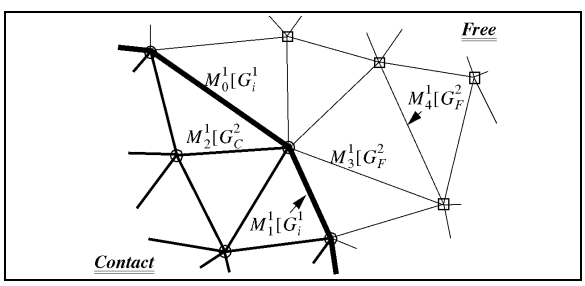

Figure 3. Classifying boundary mesh edges

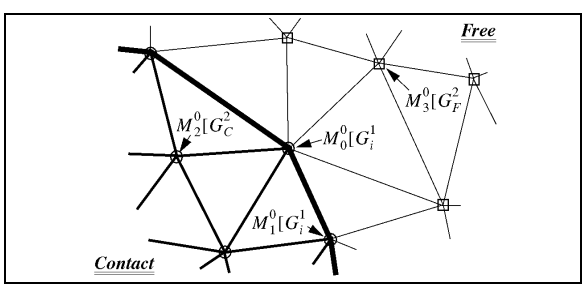

Figure 4. Classifying boundary mesh vertices

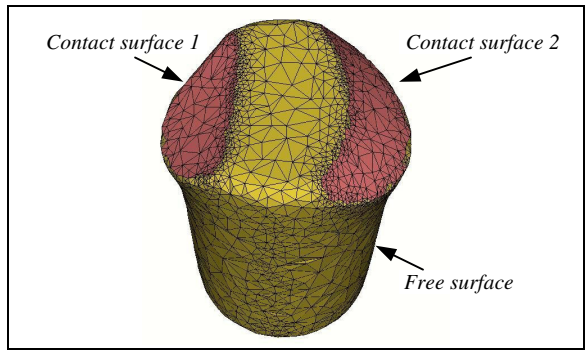

Figure 5: A mesh model for deformed object

4. MESH SIZE FIELD SPECIFICATION

Mesh discretization errors arise from the use of a finite dimensional solution space defined in terms of polynomial basis functions over a set of mesh entities. When the order of the polynomial basis function approximation is fixed, these errors directly depend on the mesh size and vanish as the mesh size approaches zero. Accordingly, these errors can be controlled by employing an *h*-adaptive analysis process when the mesh size is controlled through the domain. In this study, a mesh size field is built using error indicators and processed to control geometric approximation errors.

4.1 Error Indicators

A recovery-based *a posteriori* procedure developed by Zienkiewicz and Zhu (ZZ) [15] is used. The recovered solution is obtained based on the projection of effective strain field and is adopted to replace the exact solution in obtaining the element error indicators. The error $\|e_\varepsilon\|_\tau$ for an element τ is given in L_2 error norm by

$$\| e_\varepsilon \|_\tau = \left(\int_{\Omega_\tau} (\varepsilon - \varepsilon_h)^2 d\Omega \right)^{\frac{1}{2}} \tag{1}$$

where ε and ε_h are respectively the exact value and the finite element approximation of effective strain. Since ε is unknown, an "improved" solution ε^* is obtained by the recovery procedure and used as an indicator of the elemental error $\| e_\varepsilon \|_\tau$:

$$\| e_\varepsilon \|_\tau \approx \| e_\varepsilon^* \|_\tau = \left(\int_{\Omega_\tau} (\varepsilon^* - \varepsilon_h)^2 d\Omega \right)^{\frac{1}{2}} \tag{2}$$

For a given domain Ω', the error norm is estimated as:

$$\|e_\varepsilon\|_{L_2} \approx \left(\sum_{\tau=1}^{n} \|e_\varepsilon\|_\tau^2 \right)^{\frac{1}{2}} \tag{3}$$

where n is the total number of the elements within the domain Ω'. Furthermore, the error can be interpreted by taking the relative percentage error η defined as:

$$\eta = \frac{\|e_\varepsilon\|}{\|\varepsilon^*\|} \times 100\% \tag{4}$$

where $\|\varepsilon^*\|$ is the corresponding norm of the recovered solution over the domain Ω'.

4.2 An H-Adaptive Procedure

Based on the element error indicators and convergence rate of the finite element method, the mesh adaptivity can be readily performed to satisfy certain mesh optimality criteria. A general requirement is to ensure a minimum percentage error in certain (energy or L_2) norm to be achieved so that

$$\eta \le \hat{\eta} \tag{5}$$

is met, where $\hat{\eta}$ is the maximum allowed relative percentage error.

The optimal mesh will have the same contribution from each element to the total error. Adopting an *h*-adaptive method, the desired size of the elements in the new mesh is defined by:

$$h_\tau^{new} = h_\tau^{old} \times r_\tau \tag{6}$$

where h_τ^{old} and h_τ^{new} denote the current characteristic size of an element τ and the expected characteristic size of the new elements inside the subdomain covered by element τ, respectively. The element size factor r_τ is computed from the estimated element errors based on the following equation [16]:

$$r_\tau = \|e_\varepsilon\|_\tau^{-\frac{2}{2p+d}} \left(\frac{\hat{\eta}^2 \|\varepsilon^*\|^2}{\sum_{i=1}^{n} \|e_\varepsilon\|_i^{\frac{2d}{2p+d}}} \right)^{\frac{1}{2p}} \tag{7}$$

where d and p are respectively the dimension and order of the elements. In this study, $d = 3$ and $p = 1$.

Figure 6 shows an input mesh and an adapted mesh. As can be seen from the figure, a finer mesh is obtained where the strain gradients are high.

4.3 Processing the Mesh Size Field to Control Geometric Approximations

The mesh size field is adjusted to satisfy the further requirements over the workpiece boundary mesh to reduce geometric interference (penetration) between the workpiece mesh and the die surfaces, and to control mesh gradation around small model edges and faces that are subject to substantial deformation in future steps.

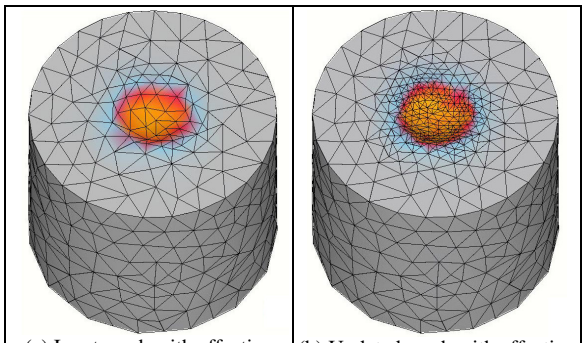

(a) Input mesh with effective strain field | (b) Updated mesh with effective strain field

Figure 6. Adaptive mesh enrichment based on error indicators for effective strain

Geometric interference (GI)

The workpiece boundary can become overlapped with the die geometries during the forming analysis [6,8,10,17]. It has been observed that an important source of geometric approximation errors due to workpiece-die overlap leads to inaccurate representation of the die-workpiece interaction and therefore results in underestimation of required forming load and overestimation of required filling material [10]. Various methods have been devised to control the overlap in the remeshing-based procedures [8,10,17]. The die-workpiece interference is generally adopted to measure the physical overlap between the workpiece and die geometries. It can be defined as $\delta = Q_W \cap Q_D$, where Q_W and Q_D represent the domains of the workpiece and dies, respectively. In order to improve the simulation results, it is desired to control the geometric interference in the updated mesh.

One of the widely used measures for quantifying the amount of δ is interference depth [8,10,17]. Generally, interference depth is defined as the minimum translational distance required to separate two overlapping objects. In forming simulations, interference depth is usually assessed as the distance from the middle point of a mesh edge with a contact node at each end to the die surface in the inner normal direction $\vec{n}_{inner}$ of the workpiece boundary at the middle point [10,17] as illustrated in Figure 7a, where ○ represents a mesh vertex in contact. Denoting the allowed interference amount as δ_p, if $\delta \ge \delta_p$ at any portion, it is regarded that the die-workpiece interference has become exceeding (too large) and needs to be reduced.

GI calculation based on examination of single location would clearly be unsuitable in the situations illustrated in Figures 7.b, c and d. The GI would be computed as zero in Figure 7b and much smaller than the actual amount in Figure 7c. For the case shown in Figure 7d where □ represents a mesh vertex not in contact, which often occurs in the incoming region, since the mesh edge M_m^1 is bounded by one free mesh vertex M_i^0 and one contact mesh vertex M_j^0, it is not considered at all. As a remedy,

in the developed procedure, interference depth is computed as the maximum value among the distances measured from multiple locations (points) along a boundary mesh edge $M_i^1[G_j^d$ of the workpiece to a die surface in the inner normal direction $\vec{n}_{inner}$ of the workpiece boundary, where $1 \le d \le 2$ and M_i^1 is bounded by 1 or 2 contact mesh vertices. This approach is illustrated in Figure 8, where 3 measuring points are taken and the computed GI is likely to be closer to the actual GI than that computed in Figure 7b and 7c. To calculate the workpiece-die distance at multiple points efficiently, a searching structure based on an octree [18] is adopted.

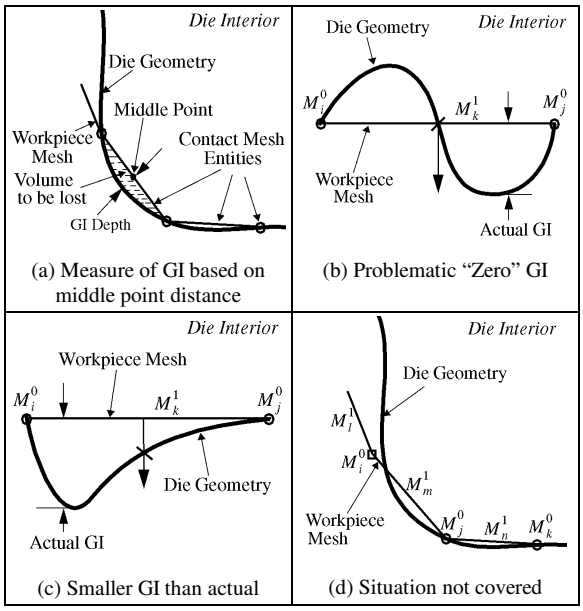

(a) Measure of GI based on middle point distance

(b) Problematic "Zero" GI

(c) Smaller GI than actual

(d) Situation not covered

Figure 7. A middle-point based GI Measure

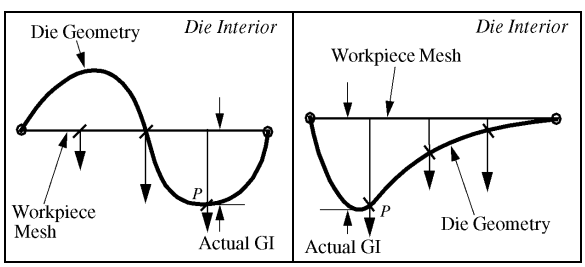

Figure 8. A 3-point based GI Measure

In such a searching procedure, an octree is built by subdividing a die surface into multiple subsurfaces recursively until each terminal octant contains a limited number of mesh faces. Denote the values $x_{\min}$, $x_{\max}$, $y_{\min}$, $y_{\max}$, $z_{\min}$ and $z_{\max}$, which satisfy the inequalities for any point $P(x, y, z)$ within a mesh face,

$$\begin{aligned} x_{\min} &\le x \le x_{\max} \\ y_{\min} &\le y \le y_{\max} \\ z_{\min} &\le z \le z_{\max} \end{aligned} \tag{8}$$

the bounding box of the mesh face is defined by two corners located at $X_{\min} = (x_{\min}, y_{\min}, z_{\min})$ and $X_{\max} = (x_{\max}, y_{\max}, z_{\max})$. For the mesh face to be contained in a terminal octant, its bounding box must reside at least partially inside the terminal octant, namely

$$\begin{aligned} x_{\min} &\le x_{o_\max} + tol \quad and \quad x_{\max} \ge x_{o_\min} - tol \\ y_{\min} &\le y_{o_\max} + tol \quad and \quad y_{\max} \ge y_{o_\min} - tol \\ z_{\min} &\le z_{o_\max} + tol \quad and \quad z_{\max} \ge z_{o_\min} - tol \end{aligned} \tag{9}$$

where, $X_{o_\min} = (x_{o_\min}, y_{o_\min}, z_{o_\min})$ and $X_{o_\max} = (x_{o_\max}, y_{o_\max}, z_{o_\max})$ represent the lower and upper corner points of the octant respectively, and $tol \ge 0$ is a tolerance defined according to the allowed GI, δ_p, in the simulation. In this study, we take $tol = 1.1 \times \delta_p$ so that only the mesh faces contained in a specific terminal octant are considered to compute the workpiece-die distance at any point $Q(x, y, z)$ that satisfies:

$$\begin{aligned} x_{o_\min} &\le x \le x_{o_\max} \quad and \\ y_{o_\min} &\le y \le y_{o_\max} \quad and \\ z_{o_\min} &\le z \le z_{o_\max} \end{aligned} \tag{10}$$

Mesh edges on the contact surfaces exceeding the allowed GI are to be refined by altering the local mesh size field to capture the local geometric features on the die surfaces. Figure 9 shows an example application of GI control.

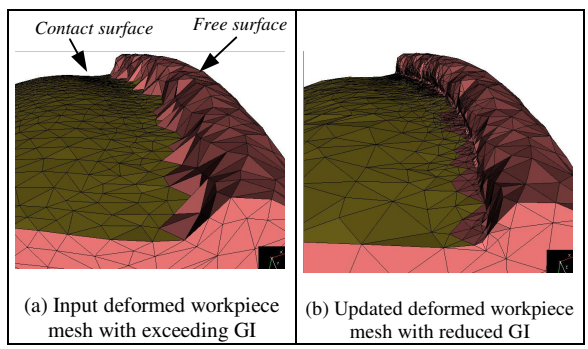

(a) Input deformed workpiece mesh with exceeding GI

(b) Updated deformed workpiece mesh with reduced GI

Figure 9. Effect of GI reduction

Mesh gradation control

When small but required model features are defined by the topology update procedure, the mesh size field around those small model features is adjusted to avoid introducing a number of poorly-shaped elements due to large mesh gradation. In the local mesh illustrated in Figure 10, there is a short model edge G_1^1 bounded by two model vertices G_0^0 and G_1^0. Denoting the length of G_1^1 as l_1 and the requested mesh size around G_1^1 as s_1. When $s_1 >> l_1$, a poorly-shaped element M_0^2 is to be introduced as shown in Figure 10a. Therefore it is desired to adjust s_1 close to l_1 so that a smooth mesh gradation is resulted as shown in Figure 10b.

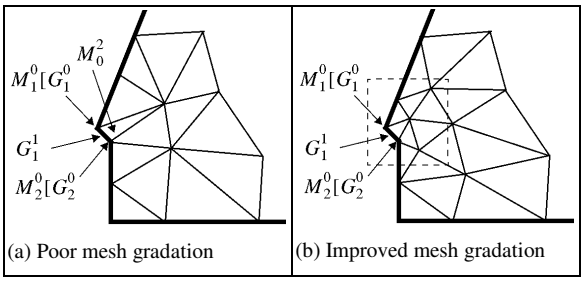

Figure 10. Mesh size adjustment for good mesh gradation

5. CONTROLLED MESH MODIFICATIONS

Adaptive mesh control is executed through the applications of local mesh modification operations.

5.1 Local Mesh Modification Operations

Before discussing the enrichment processes, the local mesh modification operations are introduced, which include:

- Splitting of mesh edges, faces and regions
- Collapsing of mesh edges, faces or regions
- Swapping of mesh edges and faces
- Geometry modification of mesh vertices, edges or faces

Splitting of mesh edges, faces and regions

The most commonly applied splitting procedure is edge splitting. In the case of simplex elements, it is straightforward to define a set of templates to account for the edge splitting in the higher order mesh entities the edge bounds [19].

Collapsing of mesh edges, faces or regions

There are a number of specific mesh entity collapsing operations that can be defined for the case of simplex elements. The most commonly applied collapsing operation is an edge collapse. The application of a requested collapsing operation is precluded if it would create a mesh invalidity [19]. Additionally, some application related geometric constraints may be applied to control the use of these operators. This will be discussed later.

Swapping of mesh edges and faces

Efforts to date on the development of mesh entity swapping procedures have been focused on simplex elements. In 3-D the swap operations are qualified and a variety of edge and face swapping operations have been defined. The application of a requested swapping operation is precluded if it would create a mesh invalidity [19].

Geometry modification of mesh vertices, edges or faces

The positions of mesh vertices and the shapes of mesh edges and faces can be altered. In all cases, there is a limit to the amount of geometric change possible before one or more connected higher order mesh entities become invalid.

5.2 Mesh Enrichment Process

Given a desired mesh size field and an expected element shape criteria for the elements, the mesh enrichments are executed by the controlled applications of local mesh modifications. Whenever either element size or shape is not satisfied, a mesh enrichment is determined and performed to eliminate the deficiency and achieve the best satisfaction of the requested size and shape.

5.2.1 Mesh entity refinement and coarsening

When an element does not satisfy the local mesh size, mesh entity refinement or coarsening, considering control of the resulting mesh entity shapes, is executed.

Mesh entity refinement is accomplished using splitting operations with edge splits being most popular due to their flexibility. It is always possible to introduce the desired mesh entity refinement in those cases where introduced mesh entities do not need to have their geometry modified. In the case where mesh entities are classified on a curved boundary of the model are split, it is necessary to modify the geometry of those mesh entities so they lie on the model boundary. These geometric modifications can invalidate the shapes of connected higher order mesh entities. In those cases additional mesh modification operators are applied to yield a valid mesh [20].

Many of the published mesh coarsening procedures are restricted to the reversal of previously executed refinement procedures. For the purposes of a more general mesh modification processes, a coarsening procedure based on mesh entity collapsing is more flexible. Edge-based collapsing procedures are well suited to most collapse needs. However, recent efforts indicate that other collapse operations are advantageous in specific circumstances. Since a specific collapsing operation may not be allowed due to its producing a mesh invalidity or large geometric approximation error, it is not always possible to execute a specific coarsening.

5.2.2 Element shape improvement

Element distortions in the workpiece mesh may cause degradation in the computed results or discontinue the simulation. Therefore, the distorted elements need to be detected and improved efficiently. The modified mean ratio, which is defined as $(15552V^2)\Big/\left(\sum_{i=1}^{6} l_i^2\right)^3$, where V is the volume of the tetrahedron and l_i is the length of i-th mesh edge bounding the tetrahedron [21], can be used to evaluate the distortion level. The distortion factor is 1.0 for an equilateral element and a value of 0.0 indicates a zero volume element. Depending upon the acceptable distortions in the FE mesh, local modifications are made to improve the shape of the distorted elements.

Mesh shape improvement efforts include node-point repositioning procedures and the application of local mesh modifications. Emphasis here is on the controlled mesh modifications.

For a poorly-shaped tetrahedral mesh region, M_i^3, rank its six bounding mesh edges, M_j^1, where $1 \le j \le 6$, by the order of their lengths squared, l_j^2, as follows:

$$l_1^2 \le l_2^2 \le l_3^2 \le l_4^2 \le l_5^2 \le l_6^2 \tag{11}$$

When $l_1^2 << l_6^2$, the poor shape of M_i^3 is due to the existence of "short" mesh edge(s), otherwise it must contain large dihedral angles. Figure 11 shows examples of poorly shaped elements taking the various configurations. Figures 11a and 11b have the case of a short mesh edge, $M_{j_0}^1$. Figure 11c is the case of two large dihedral angles and Figure 11d is the case of three large dihedral angles. Accordingly, application of mesh modifications is guided by the two basic goals of:

- Removal of poorly-shaped mesh regions which contain "short" mesh edge(s) through elimination of those "short" mesh edges;
- Removal of the large dihedral angles based on operators keyed by the ordered mesh edge lengths and the adjacency information.

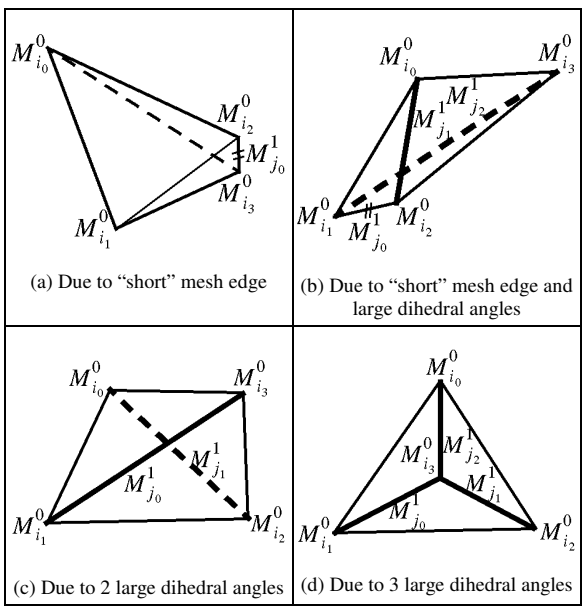

Figure 11. Poor element shape due to "short" edge(s) and/or large dihedral angle(s)

Handling mesh regions containing "short" mesh edge(s)

The options to eliminate a "short" mesh edge include collapsing it by removing either its bounding mesh vertex, an appropriate swap operation, or repositioning its bounding mesh vertices. The topological restrictions on edge collapsing are discussed in detail by Cougny and Shephard [19]. The geometric restrictions on edge collapse require that all updated mesh regions have positive volumes.

When elimination of the "short" mesh edge(s) is not allowed geometrically, alternative consideration is to remove either its bounding mesh vertex by collapsing a mesh edge that connects to it within the local mesh such that the edge is eliminated by merging with a longer edge. An example to overcome the geometric restrictions in 2D is illustrated in Figure 12, where a "short" mesh edge M_1^1 bounds two poorly-shaped elements (mesh faces), M_1^2 and M_2^2 (Figure 12a). The first attempt is naturally to collapse M_1^1 with the mesh vertex M_1^0 deleted as shown in Figure 12b. However this leads to definition of an invalid mesh face M_3^2 which are bounded by mesh vertices M_2^0, M_4^0 and M_6^0, and therefore is not allowed geometrically. As an alternative, one of the mesh edges connected to M_1^1 at M_1^0 can be collapsed with M_1^0 deleted. In Figure 12c, mesh edge M_2^1 is collapsed and in Figure 12d, mesh edge M_5^1 is collapsed. Both these operations are allowed geometrically. The modification by collapsing M_5^1 (Figure 12d) leads to the better local mesh quality and thus is selected to be applied.

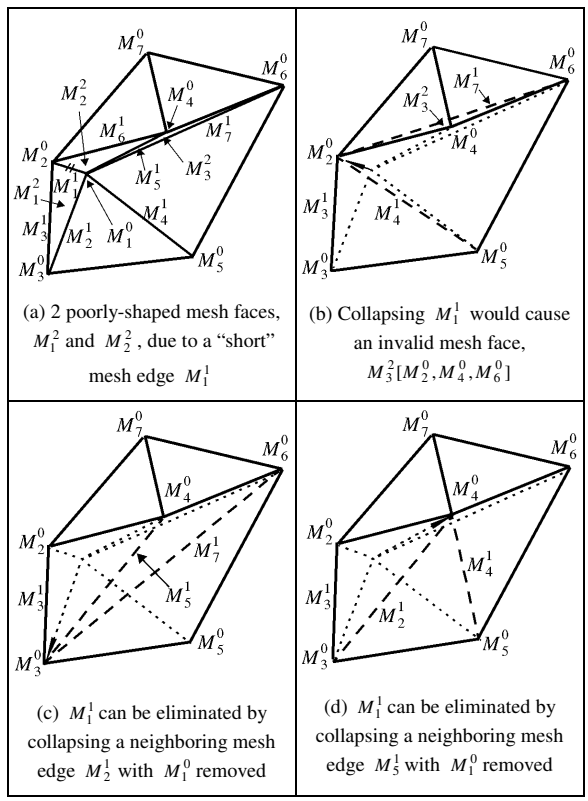

Figure 12. Eliminate a "short" mesh edge by overcoming geometric restrictions

Handling mesh regions containing large dihedral angle(s)

A poorly-shaped mesh region containing no "short" mesh edges must contain one to three large dihedral angles. Considering the possible effects on the local mesh, a simple deletion is preferred. Some of the cases when these elements arise happen when a flat mesh region has one or more mesh faces classified on a model face that is used by only one model region with the remaining mesh faces classified in that model region. In these cases, the mesh region can simply be deleted with the remaining mesh faces and model region classified mesh edges and vertices reclassified on the model face on which the deleted face(s) were classified.

When a mesh region containing large dihedral angle(s) can not be removed by a simple deletion, the situation needs to be analyzed based on the adjacency information to determine the most desired mesh modification to eliminate as many large dihedral angles as possible. Consider the case shown in Figure 11d, where mesh edges, $M^1_{j_0}$, $M^1_{j_1}$ and $M^1_{j_2}$, bounded by mesh vertex $M^0_{i_3}$, are the three shortest mesh edges within element M^3_i. It is possible to eliminate all potential large dihedral angle(s) by collapsing one of these three mesh edges as shown in Figure 13a. If none of these mesh edges, $M^1_{j_0}$, $M^1_{j_1}$ and $M^1_{j_2}$, can be collapsed, an additional effort is to look at the shapes of the mesh faces bounded by them within the element, and to swap the longest mesh edge bounding a sliver mesh face if there exists one. The situation is illustrated in Figure 13b, where mesh face $M^2_{k_0}$ bounded by mesh edges $M^1_{j_0}$, $M^1_{j_1}$ and $M^1_{j_3}$ is sliver, and the mesh edge $M^1_{j_3}$ is considered to be appropriately swapped.

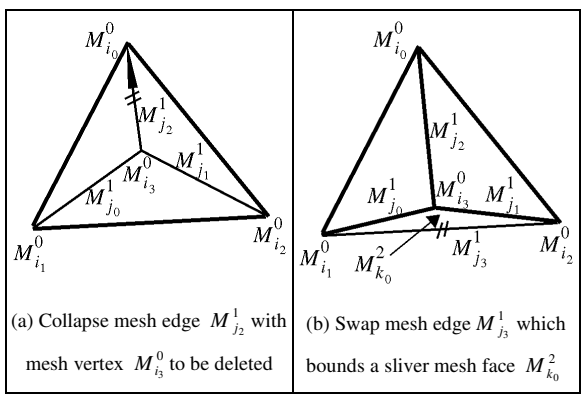

(a) Collapse mesh edge $M^1_{j_2}$ with mesh vertex $M^0_{i_3}$ to be deleted

(b) Swap mesh edge $M^1_{j_3}$ which bounds a sliver mesh face $M^2_{k_0}$

Figure 13. Part of efforts to remove a poorly-shaped element with 3 large dihedral angles

5.3 Geometry Shape Updates

During the mesh enrichment process, the contact and free surfaces of the workpiece are carefully maintained through geometry shape updates to reduce geometric approximation errors.

Treatment on new contact mesh vertices

A situation that requires specific consideration is when boundary mesh edges are split. In these cases, the new contact mesh vertices geometrically not on specific die surfaces and other new mesh vertices inside die surfaces need to be placed on the die surfaces as illustrated in Figure 14. Repositioning of the new mesh vertices is conducted through a vertex snapping procedure [20].

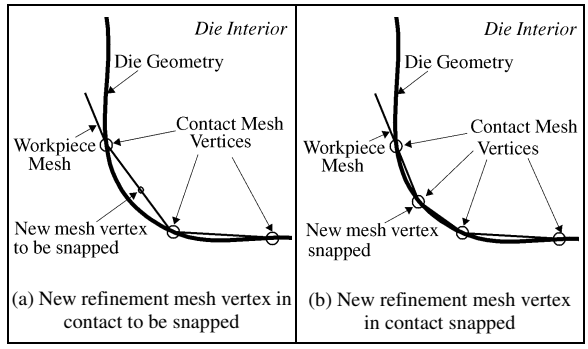

(a) New refinement mesh vertex in contact to be snapped

(b) New refinement mesh vertex in contact snapped

Figure 14. Snapping of new contact refinement mesh vertices

Free surface smoothing

It has been observed that in cases where the mesh used is not a good approximation to the smooth geometry of the workpiece free surfaces, the simulation accuracy can degrade [3]. Subdivision surface procedures can be adopted during refinement of the free surfaces to approximate the actual surface curvature. In the developed procedure, the position of the subdivision points along the boundary mesh edges are calculated in the form of interpolation functions through employing a modified butterfly scheme [22,23]. The interpolation templates to be applied are selected based on the mesh entity classification and the adjacency around the mesh edges in the local boundary mesh.

5.4 Local Transfer of History Dependent Solution Information

Operations like remeshing or local mesh modifications require the history-dependent solution fields be accurately transferred from the original mesh to the modified mesh so that the computation can be resumed and continued from the updated reference state. When the deformed mesh is updated through a local mesh modification operation, the solution fields for only the involved local mesh need to be transferred.

There are two methods used to transfer solution parameters. They involve using a) the existing interpolants or b) new interpolants defined to satisfy certain desired properties. Since only the solution information over the modified local mesh is transferred depending on individual local mesh modifications, the required calculations are local and efficient.

6. INDUSTRIAL APPLICATIONS

A back extrusion problem and a steering link problem are investigated to demonstrate the capabilities developed in this study. To show the improvements achieved, both of the problems are solved by using DEFORM only and the automated mesh modification procedure (which uses DEFORM as FEM engine) and the solutions are compared. Results obtained are presented and discussed below.

6.1 A Back Extrusion Problem

A back extrusion problem shown in Figure 16 is considered. The plastic behavior of the material is specified with a material flow stress function. A total stroke of 7.2 inches is defined, which corresponds to 180 steps with a stroke of 0.04 inch per step. The allowed geometric interference is 0.07 inch. The initial mesh of workpiece consists of 906 mesh vertices and 5433 mesh regions.

The problem is solved by 1) using DEFORM's remeshing procedure and 2) using the automated mesh modification procedure. The simulation requires 13 DEFORM's remeshings and 9 mesh enrichment steps, respectively (see Table 1).

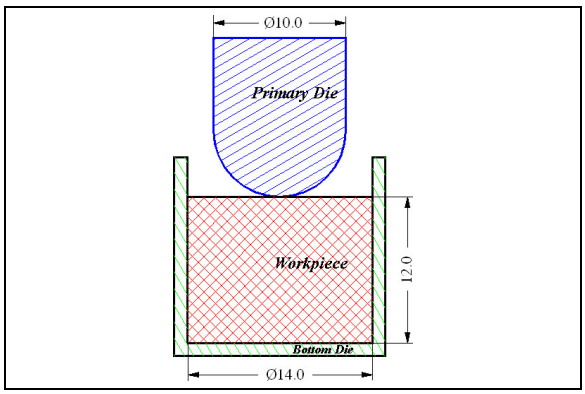

Figure 16. A Back Extrusion Problem

Table 1: Remeshings and Mesh Enrichments used

Remeshings	At Step	Number of Elements	Mesh Enrichments	At Step	Number of Elements
1	5	10049	1	5	7041
2	12	10834			
3	22	10763	2	19	10575
4	26	14171			
5	41	21158			
6	52	21605	3	50	10890
7	65	21754	4	72	13077
8	81	21727			
9	92	23242	5	99	14246
10	112	24698	6	120	17952
11	134	24599	7	133	25219
12	154	25272	8	155	30325
13	166	24771	9	172	38136

In Figure 17 the maximum dihedral angles of the workpiece mesh are compared before and after the remeshings and the mesh enrichments, respectively. It can be seen the mesh quality is stably and largely improved through the mesh enrichments, particularly during the later stages of the simulation.

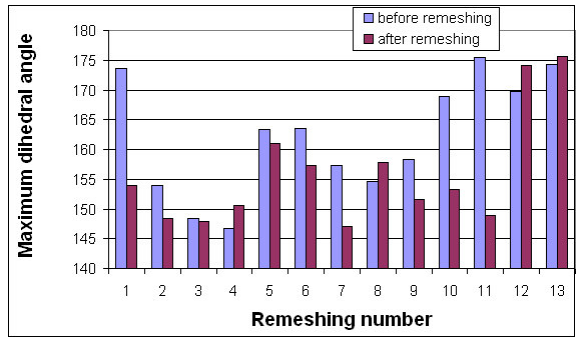

(a) By remeshings

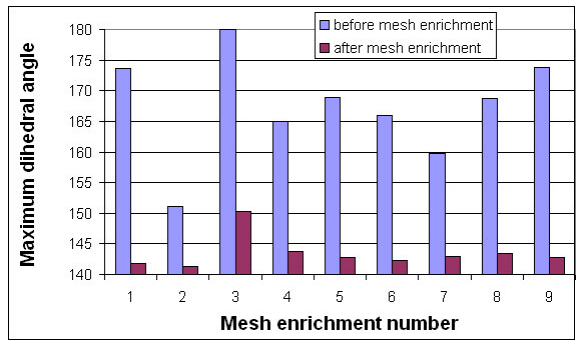

(b) By mesh enrichments

Fig 17. Changes of the maximum dihedral angles before and after remeshings/mesh enrichments

A temperature field updated by the local mesh modification dependent solution transfer operators is shown in Figure 18. As can be seen, solution transfer does not lose any significant information. As expected, the global transfer demonstrated a greater diffusion of peak values.

Four steps of the simulation process are given in Figure 19. From the figure, it can be seen that the contact surface between the moving die and the workpiece is well captured by controlling the workpiece-die geometric interference. Furthermore, it can be observed that high mesh density is obtained around high strain gradient regions, which are in the vicinity of moving die surface.

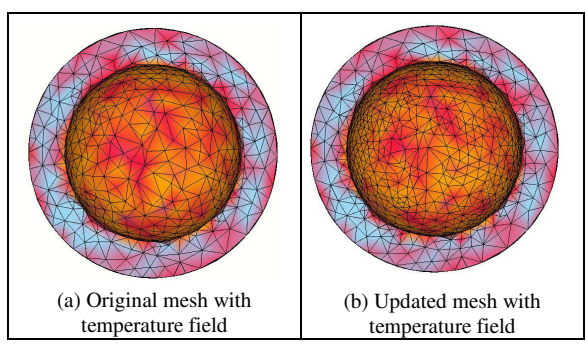

(a) Original mesh with temperature field

(b) Updated mesh with temperature field

Figure 18. Updated temperature field by local transfer operators

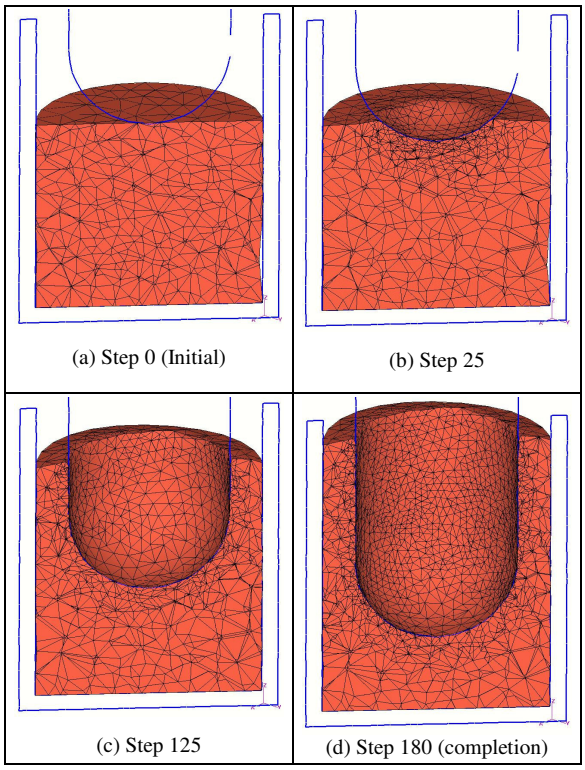

Figure 19. Interior workpiece mesh produced by automated mesh modification procedure

6.2 A Steering Link Problem

A steering link problem shown in Figure 20 is considered. The plastic behavior of the material is specified with a material flow stress function. A total stroke of 41.7mm is defined, which corresponds to 278 steps with a stroke of 0.15mm per step. The allowed geometric interference is 1.0mm. The initial workpiece mesh consists of 6765 mesh vertices and 28885 mesh regions.

The problem is solved respectively by 1) DEFORM's remeshing procedure and 2) the mesh modification procedure. The first remeshing/mesh enrichment is needed at STEP 112. It takes 35 DEFORM's remeshings and 18 mesh modification steps.

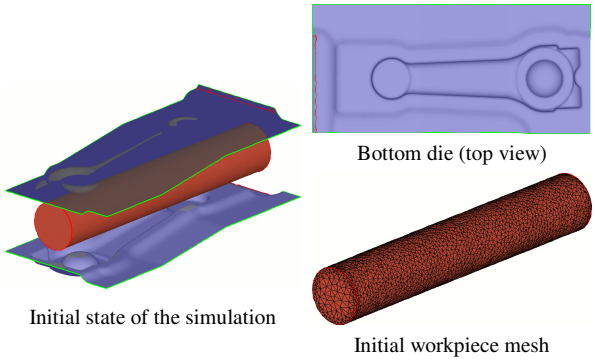

Figure 20. Setup of a steering link problem

Improvements of element quality

The quality of the workpiece mesh is improved stably by the mesh enrichments through the entire simulation process. Figure 21 shows the improvements to the maximum dihedral angles before and after the mesh enrichments.

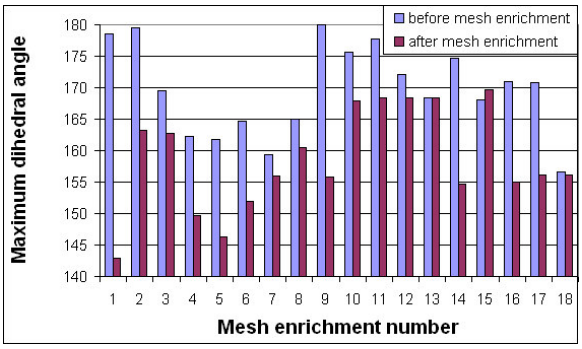

Figure 21. Element quality improved through mesh enrichments

Mesh size control

The workpiece mesh is adapted to control solution error and the geometric approximation. The maximum edge length increases from 11.98mm in the initial mesh to 24.49mm in the final mesh while the minimum edge length decreases from 0.92mm to 0.30mm. The effects of mesh adaptivity are shown in Figure 22.

The interior mesh density and effective strain of the final workpiece mesh are compared between the adaptive enrichment based and the remeshing based simulations as shown in Figure 23.

The simulation ends with a final mesh containing 24729 mesh vertices and 115483 mesh regions. The estimated relative error in effective strain decreases from 11.69% at STEP 112 to 6.53% at the end. The final mesh is compared with the one obtained by DEFORM's remeshings in Figure 24.

7. CLOSING REMARKS

This paper has considered an automated adaptive mesh control procedure for metal forming simulations. The adaptive mesh control is executed through the controlled applications of mesh modification operators, which are based on an adaptively defined mesh size field. To properly maintain the workpiece boundary conditions, the model topology of the workpiece mesh is updated consistently with the solution information. The mesh size field is obtained by accounting for discretization errors through an *h*-adaptive procedure guided by error indicators and procedures to control the geometric approximations.

The adaptive mesh modifications are applied to two 3-D forming problems and compared with a procedure that employs complete remeshings. The results demonstrate the ability of adaptive mesh modification procedures to

properly deal with any of the complications that can arise during the simulation. Mesh modification based adaptive procedures have also been applied to transient flow simulations including ones with bodies in relative motion.

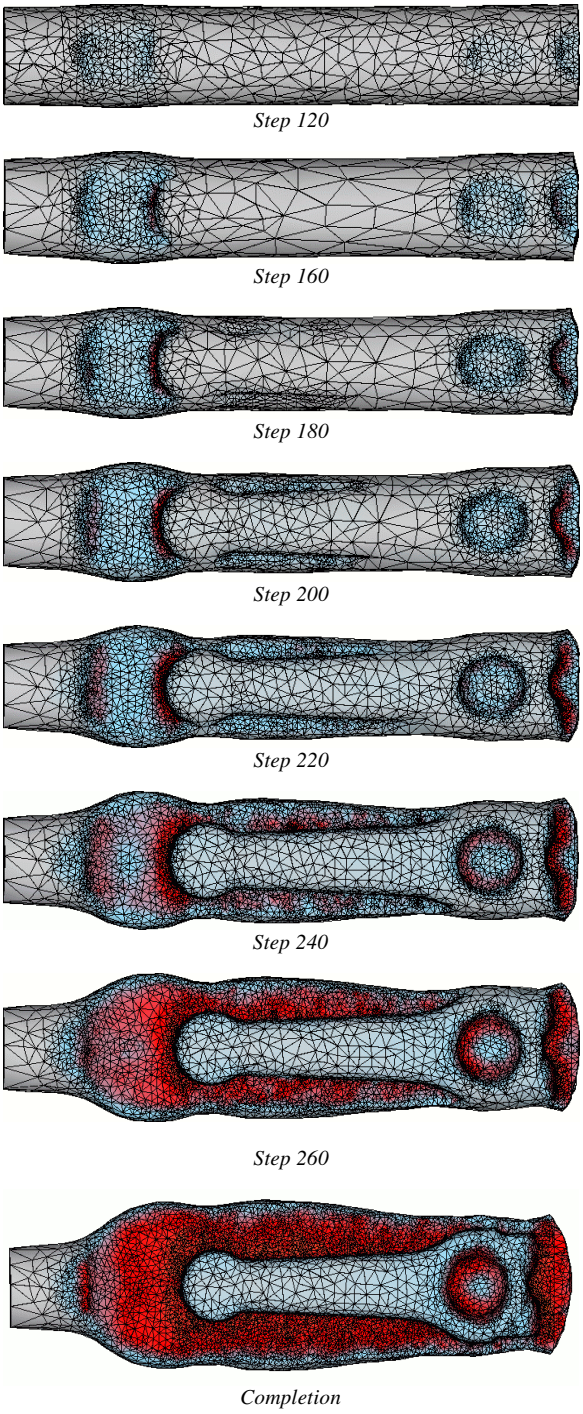

Figure 22. Mesh adapted consistently with the effective strain profile

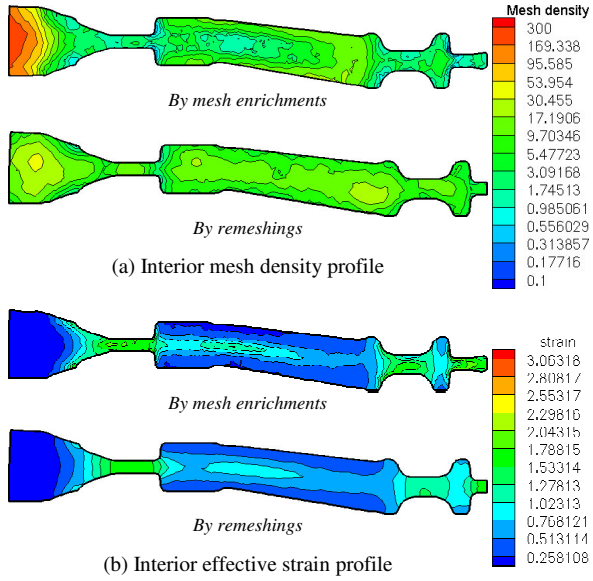

(a) Interior mesh density profile

(b) Interior effective strain profile

Figure 23. The final interior mesh density and effective strain profiles

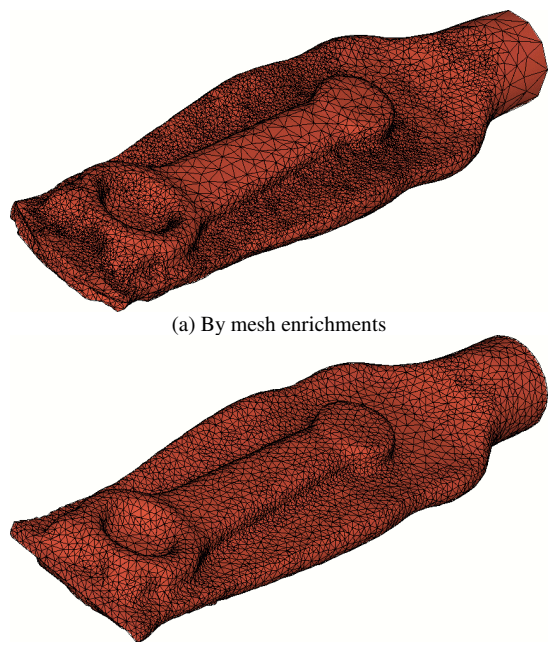

(a) By mesh enrichments

(b) By remeshings
(12046 mesh vertices and 51987 mesh regions)

Figure 24. Final meshes of the workpiece

REFERENCES

[1] J. H. Cheng and N. Kikuchi, "A Mesh Rezoning Technique for Finite Element Simulation of Metal Forming Processes", *International Journal for Numerical Methods in Engineering*, Vol. 23, pp. 219-228 (1986)

[2] A. Habraken and S. Cescotto, "An Automatic Remeshing Technique for Finite Element Simulation of Forming Processes", *International Journal of Numerical methods for Engineering*, Vol. 30, pp. 1503-1525 (1990)

[3] N. V. Hattangady, M. S. Shephard and A. B. Chaudhary, "Towards Realistic Automated 3D Modelling of Metal Forming Problems", *Engineering with Computers*, Vol. 15, pp. 356-374 (1999)

[4] M. N. Ravindranath and R. K. Kumar, "Simulation of Cold Forging using Contact and Practical Adaptive Meshing Algorithms", *Journal of Material Process Technology*, vol. 104, pp. 110-126 (2000)

[5] Ch. P. Chand and R. K. Kumar, "Remeshing issues in the finite element analysis of metal forming problems", *Journal of Material Processing Technology*, vol. 75, pp. 63-74 (1998)

[6] Y. Y. Zhu, T. Zacharia and S. Cescotto, "Application of Fully Automatic Remeshing to Complex Metal-forming Analyses", *Computers and Structures*, vol. 62, No. 3, pp. 417-427 (1997)

[7] K. M. Mathisen, O. S. Hopperstad, K. M. Okstad and T. Berstad, "Error Estimation and Adaptivity in Explicit Nonlinear Finite Element Simulation of Quasi-static Problems", *Computers and Structures*, Vol. 72, pp. 627-644 (1999)

[8] D. Y. Kwak, J. S. Cheon and Y. T. Im, "Remeshing for Metal Forming Simulations. Part I: Two-dimensional Quadrilateral Remeshing", *International Journal for Numerical Methods in Engineering*, Vol. 53, pp. 2463-2500 (2002)

[9] T. Coupez, "Automatic Remeshing in Three-dimensional Moving Mesh Finite Element Analysis of Industrial Forming", *in S. F. Shen and P. R. Dawson (editors), Simulation of Material Processing: Theory, Practice, Methods and Applications, Balkema, Rotterdam*, pp. 407-412 (1995)

[10] DEFORM 3D™ User Manual, SFTC, Colubus, OH.

[11] S. Kobayashi, S-I OH and T. Altan, "Metal Forming and the Finite Element Method", Oxford University Press, New York (1989)

[12] P. L. George, "Automatic Mesh Generation. Reading", MA, Addison-Wisley (1991)

[13] M. S. Shephard, P. L. Baehmann, R. R. Collar, N. V. Hattangady and Q. Niu, "Automated Remodeling Techniques in Finite Element Analysis", Advances in CAD/CAE, Academic Press (1993)

[14] M. W. Beall and M. S. Shephard, "A General Topology-based Mesh Data Structure", *International Journal for Numerical Methods in Engineering*, Vol. 40, 1573 (1997)

[15] O. C. Zienkiewicz and J. Z. Zhu, "The Superconvergent Patch Recovery and A Posteriori Error Estimates. Part 1: The Recovery Technique", *International Journal for Numerical Methods in Engineering*, v. 33, p. 1331-1364 (1992)

[16] M. Braack, R. Becker and R. Rannacher, "An Adaptive Finite Element Method for Combustion Problems", *Proceedings of the Third Summer Conference, Numerical Modelling in Continuum Mechanics, Charles Universirt, Prague*, (1997)

[17] N. V. Hattangady, "Automatic Remeshing in 3-D Analysis of Forming Process", *International Journal of Numerical methods for Engineering*, Vol. 45, pp. 553-568 (1999)

[18] M. S. Shephard and M. K. Georges, "Automatic three-dimensional mesh generation by the finite octree technique", *International Journal for Numerical Methods in Engineering*, v 32, n 4, pp. 709-749 (1991)

[19] H.L. de Cougny and M.S. Shephard, "Parallel Refinement and Coarsening of Tetrahedral Meshes", *International Journal for Numerical Methods in Engineering*, Vol. 46, pp. 1101-1125 (1999)

[20] X. Li, M. S. Shephard and M. W. Beall, "Accounting for Curved Domains in Mesh Adaptation", *International Journal for Numerical Methods in Engineering,* in press.

[21] A. Liu and B. Joe, "Relationship between tetrahedron shape measures", *BIT*, Vol. 34, pp. 268-287 (1994)

[22] D. Zorin, P. Schroder and W. Sweldens, "Interpolating Subdivision with Arbitrary Topology", *Proceedings of Computer Graphic, ACM SIGGRAPH*, pp. 189-192 (1996)

[23] C. K. Lee, "Automatic Metric 3D Surface Mesh Generation using Subdivision Surface Geometrical Model. Part I: Construction of Underlying Geometric Model", *International Journal for Numerical Methods in Engineering*, Vol. 56, pp. 1593-1614 (2003)